Sound & Vibration 2026, 60(3), 4129.
doi: https://doi.org/10.59400/sv4129

Article

Non-contact full-field vibration measurement using 3D digital image correlation: Experimental validation against accelerometers in multi-axis dynamic testing

Suleiman Ibrahim Mohammad[1,*], **Asokan Vasudevan**[2], **Seif Al Bustanji**[3]

[1] Research Fellow, INTI International University, Nilai 71800, Malaysia

[2] Faculty of Business and Communications, INTI International University, Nilai 71800, Malaysia

[3] Faculty of Technical Education, Hourani Center for Applied Scientific Research, Al-Ahliyya Amman University, Amman 19328, Jordan

*** Corresponding author:** Suleiman Ibrahim Mohammad, dr_sliman@yahoo.com

CITATION

Mohammad SI, Vasudevan A, Al Bustanji S. Non-contact full-field vibration measurement using 3D digital image correlation: Experimental validation against accelerometers in multi-axis dynamic testing. Sound & Vibration. 2026; 60(3): 4129. https://doi.org/10.59400/sv4129

ARTICLE INFO

Received: 6 March 2026
Revised: 10 April 2026
Accepted: 15 April 2026
Available online: 5 June 2026

Abstract: Accurate measurement of such vibrations is a prerequisite for any research work in the field of structural dynamics, modal analysis, and evaluation of machinery reliability. Although accelerometers are traditionally used for experimental vibration analysis, their use is also associated with certain limitations such as mass loading effects and under-sampling issues. Non-contact full-field vibration measurement techniques such as three-dimensional digital image correlation (3D-DIC) have also emerged as potential alternatives for vibration measurement. However, their comprehensive evaluation for full-field vibration measurement under broadband random excitations is still limited. This paper presents an experimental evaluation of the full-field vibration measurement technique using 3D-DIC for vibration measurement. The performance evaluation of the technique is also carried out using a conventional vibration measurement technique such as accelerometers. A ribbed aluminium cantilever plate is subjected to controlled broadband random excitations, and the vibration response is measured using a stereo high-speed full-field vibration measurement technique such as 3D-DIC and a triaxial accelerometer. The comparative analysis showed considerable concurrence between the two systems in the assessment of the displacement amplitude tracking, resonance identification, and modal shape characterization. Statistical evaluation showed the absence of any statistically significant difference in the mean displacement measurement within the established industrial tolerance limit. The optical system provided continuous spatial resolution and multi-axis displacement mapping without the application of any structural mass loading. This shows the equivalence and the industrial applicability of the 3D-DIC method for broadband multi-axis dynamic testing, thus making it suitable for the analysis of the vibration behaviour of the structure.

Keywords: 3D digital image correlation; full-field vibration measurement; multi-axis dynamic testing; frequency response function; modal analysis; measurement uncertainty; structural dynamics validation

1. Introduction

Accurate vibration measurements remain a vital element in the field of structural dynamics, machinery reliability, and qualification tests. Experimental modal analysis, as a tool for vibration analysis, heavily depends upon estimating frequency response functions, identifying modal parameters, and measuring displacement amplitudes for

the purpose of model validation and failure prevention. Piezoelectric accelerometers have traditionally remained the main tool for performing measurements, considering their robustness, wide frequency response, and standardized calibration [1, 2]. However, despite the popularity and wide applicability of accelerometers, some inherent disadvantages have remained, particularly for lightweight and thin-walled structures, considering the influence that the sensor might have on the local dynamic response [3]. The influence of the sensor, or mass loading, has previously demonstrated its effects upon the modal frequencies and mode shapes for sensitive structures. The discrete placement of accelerometers has also limited the resolution, and interpolation techniques have had to be employed for obtaining continuous fields [3].

In response to these limitations, non-contact optical measurements have received growing interest from scholars. Digital Image Correlation (DIC) has been identified as an effective method for measuring displacements on the entire surface of an object without making physical contact with the object. The theoretical basis of DIC is extensively discussed [4]. Afterward, DIC has been used to measure displacements during dynamic processes. The initial studies on DIC for dynamic measurements showed promise but were limited by certain limitations related to resolution and noise [5]. With recent advances in high-speed cameras and correlation algorithms, DIC systems have shown improved accuracy for measuring vibrations [6]. One of the main differences between the signal processing of accelerometer-based displacement estimation and optical displacement measurement is based on their signal processing paths. Displacement estimated through accelerometers requires double integration of the acceleration signals, given by the equation

$$X(\omega) = \frac{A(\omega)}{-\omega^2}$$

which leads to a frequency-dependent increase of uncertainty levels, particularly at low frequencies [7]. Conversely, the displacement measured through optical sensors is directly measured without any drift associated with double integration. However, uncertainty associated with the pixel resolution of the optical sensors is a unique feature of uncertainty associated with this measurement technology [8, 9]. The viability of using DIC for vibration measurement has been established. However, a large number of published research works focused on the measurement of vibration under narrowband excitation, uniaxial vibration characterization, and simple structures. A comprehensive validation methodology that considers broadband excitation, characterization of multi-axis responses, correlation of modal shapes, hypothesis tests, and propagation of uncertainties is rather limited. In addition, comparative validation of rib-stiffened structures or structurally coupled systems, which are often used to simulate real-world scenarios, has been insufficiently discussed. It is a well-known fact that the multi-axis dynamic behaviour, including the coupling of bending-torsion modes, plays a vital role in the characterization of stiffened structures [10].

2. Literature review

The conventional experimental vibration analysis techniques were based on contact sensing modalities, with piezoelectric accelerometers being the dominant measurement tools for structural characterization and modal identification. Grounded modal testing methodologies were developed [11] that primarily focused on the accelerometer-based measurement technique to measure frequency response functions (FRFs) to identify modal characteristics. These methodologies were proved to be reliable and reproducible within a controlled experimental setup. For example, the conventional accelerometer-based measurement technique was recognized to be limited for structures with low masses, as the underlying measurement tool was recognized to affect the modal characteristics of the structure. For example, the conventional accelerometer-based measurement technique was recognized to be limited for structures with low masses, as the underlying measurement tool was recognized to affect the modal characteristics of the structure.

The digital image correlation (DIC) technique has now gained recognition as a tool for measuring displacement and strain without making contact with the object under observation. The concept of digital image correlation, which is now widely recognized as a tool for quasi-static deformation analysis, has been thoroughly explored [12], wherein the theoretical background for subset-based correlation for the estimation of full-field displacement has been presented. The use of digital image correlation has traditionally been limited to quasi-static deformation analysis, as the camera speed has been a major constraint for its use in dynamic analysis. Murray et al. [5] have explored the use of stereo-digital image correlation for the estimation of the vibration of thin plates, which, although a successful experiment, has also demonstrated the limitations that have traditionally plagued the use of digital image correlation for dynamic analysis, including the sensitivity of the results to noise. Hagara and Huňady [13] have further explored the use of digital image correlation for dynamic analysis, which has demonstrated that the results obtained from correlation analysis have a tendency to deteriorate with high-frequency motions.

Significant developments have been observed in high-speed imaging technology and processing capabilities, which have widened the scope of digital image correlation (DIC) in the field of structural dynamics. Trebuňa et al. [14] showed that high-speed image correlation can be used to measure the modal response of structures with frequency ranges beyond several hundred hertz with acceptable accuracy. Liu et al. [15] have improved the stereo calibration and correlation algorithms, which have resulted in an increase in the precision of measurement. All these developments have moved the technology of optical full-field measurement from the laboratory to the testing of vibration. Several studies have compared the capabilities of digital image correlation with other measurement technologies, but most of them have considered harmonic and one-axis vibration testing.

Displacement amplitude accuracy has traditionally been a key issue in the validation of vibration data. According to Neumayer and Bretterklieber [16], displacement measured using accelerometers requires the double integration of

acceleration signals, which is associated with a frequency-dependent amplification of uncertainty. This is because of the inverse square relationship between uncertainty and angular frequency. The potential for low-frequency noise is a major concern in this context. Comparison studies involving laser vibrometers and accelerometers have reported differences caused by sensitivity to integration uncertainty, particularly at low frequencies [17]. In contrast, digital image correlation systems directly measure displacement without the need for double integration of signals, thus avoiding the associated frequency-dependent amplification of uncertainty. However, a new source of uncertainty is introduced by the pixel resolution of the optical systems, as discussed by Ben-Aryeh [18].

Another significant variable in the validation of the dynamics was the estimation of the frequency response function (FRF). Saunders [11] emphasized that a reliable estimation of the frequency response function is largely dependent on the choice of estimators and evaluation of the coherence. Although there was a promising indication of the consistency of the results in terms of the magnitude of the frequency response function, as revealed in the experimental studies [19] using the optical methods, the validation of the results in terms of the phase and wideband coherence analysis was limited. Besides, there were a few studies that examined the consistency of the results in terms of the frequency response function, modal shapes, and statistical hypothesis testing in a combined manner.

Modal parameter identification and correlation of mode shapes are two areas of major concern in experimental modal analysis. The Modal Assurance Criterion (MAC), proposed as a component of the modal validation field and thoroughly discussed by Richardson et al. [20], provides a quantitative criterion for mode shape similarity. It has been demonstrated that a sparsely arranged array of accelerometers can limit spatial resolution, possibly resulting in a reduced estimation of curvature gradients or torsion coupling [21]. Full-field optical measurements offer a potential improvement in spatial resolution and curvature estimation capabilities, as recently demonstrated within experimental studies on structures [22]. Bending-torsion coupling effects were shown [23] to significantly affect modal responses for stiffened plate structures. While tri-axial accelerometers offer local responses in multiple directions, there is limited inherent ability to create three-dimensional displacement fields. Stereo-DIC systems possess theoretical capacity to capture simultaneous responses in multiple directions, although limited empirical validation of this capacity for broadband responses is reported.

Conceptual model

The conceptual framework (**Figure 1**) was designed based on the core assumption that three-dimensional digital image correlation (3D-DIC) can provide a full-field displacement response that is metrologically equivalent to that obtained with conventional accelerometers, as long as the test conditions are controlled and the measurements are synchronized. In the model, the phenomenon under consideration is the vibration response of the rib-stiffened cantilever plate, and the two measurements are considered as parallel systems observing the same reality.

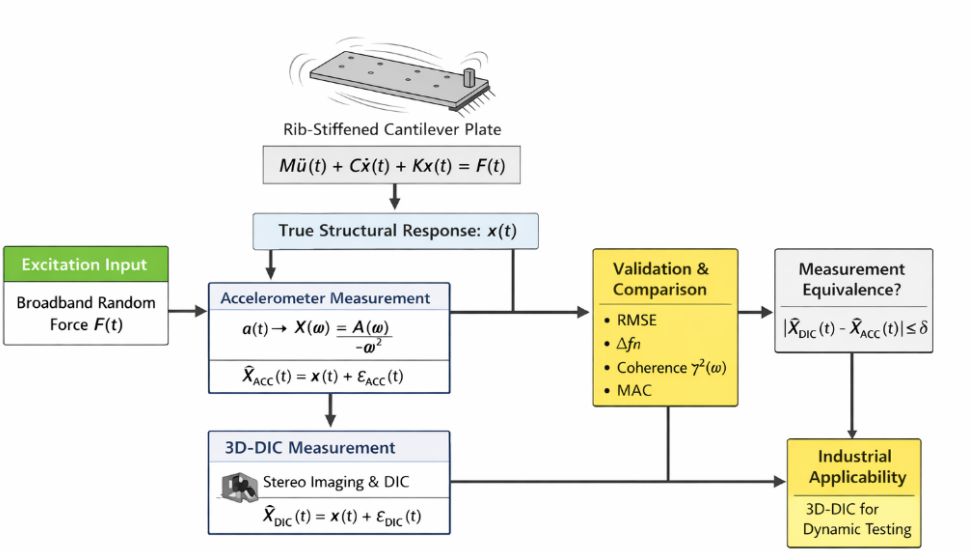

Figure 1. Conceptual Model of Measurement Equivalence and Validation Pathway.

In this context, the input signal for excitation, described by a broadband random force input via an electrodynamic shaker, functioned as the main stimulus to induce a structural response described by a displacement field along multiple axes. The response was measured by two simultaneous input channels. First, tri-axial accelerometers measured acceleration responses at fixed points, from which displacement was indirectly measured by spectral domain integration of the acceleration responses. Second, a three-dimensional digital image correlation (3D-DIC) system directly measured displacement response as a continuous spatial field across the plate's surface. The responses from the two channels were subsequently compared based on accuracy and reliability criteria defined by root-mean-square (RMS) error, similarity of the frequency response function (FRF), coherence, and modal assurance criterion (MAC).

Consequently, the conceptual model reflected a cause and measurement process, whereby the excitation led to an authentic structural response, with the results obtained from the two measurement methods reflecting estimated representations of the same response. The similarity between the results obtained from the measurements was then perceived as an indication of the validity and applicability of the non-contact method for use in industrial vibration tests. This conceptual model was consistent with the requirements for conducting hypothesis tests, as presented in the literature on research methodology. From the formal viewpoint, the conceptual model is defined as the framework for measurement equivalence. Let $x(t)$ represent the true response of the structure. The estimates provided by the measurement systems are given by:

$$\widehat{x}_{DIC(t)} = x(t) + \varepsilon_{DIC(t)}$$

$$\widehat{x}_{ACC(t)} = x(t) + \varepsilon_{ACC(t)}$$

In the design of the study, the goal was to minimize the error processes $\varepsilon_{DIC(t)}$ and $\varepsilon_{ACC(t)}$ through the process of calibration and excitation, and subsequently determine if the difference is within an acceptable level. Due to the fact that the investigation

was conducted as a hypothesis-testing experimental study, hypotheses were formulated for the evaluation of the measurements' agreement, modal faithfulness, and industrial feasibility under multi-axis dynamic excitation. Hypotheses were formulated as null and alternative hypotheses for the transparent application of statistical and engineering acceptance criteria. The main hypothesis for the evaluation of the overall equivalence of the results obtained by the two methods was that the null hypothesis stated that the mean displacement difference between the displacement obtained by the DIC method and the displacement obtained by the accelerometer method was not statistically significant for identical excitation conditions.

The alternative hypothesis stated that the mean displacement difference was statistically significant for the two methods. The second hypothesis was for the evaluation of the overall equivalence, considering the fact that the overall results obtained by the practical application of the vibration tests are based on the overall integrity of the results obtained for the resonance conditions. The null hypothesis stated that the natural frequencies obtained by the DIC and the accelerometer methods did not differ by more than the engineering tolerance. The third hypothesis was based on modal shape consistency, as full-field DIC was assumed to offer greater spatial resolution compared to point sensors. It was also assumed to be physically consistent with the same structural dynamics. The null hypothesis was that the DIC-derived modal shapes were consistent with the accelerometer-derived modal shapes with high correlation, as indicated by the MAC.

The fourth hypothesis was based on measurement reliability. It was based on the practical test of measurement reliability using the concept of coherence to determine whether the input-response relationship was linear and noise-limited. The null hypothesis was that the coherence was greater than the defined reliability threshold over the excitation bandwidth. The final hypothesis, which was based on the study's objective of ensuring the integration of measurement validation with the practical test of measurement feasibility, was based on the determination of the accuracy of the non-contact measurement. It was based on the concept of defining the problem solution based on the concept of the acceptance or rejection of the measurement. Assuming NRMSE to be the normalized RMS error.

3. Methodology

3.1. Research design

The study used a quantitative, experimental, hypothesis-testing research approach to evaluate the measurement accuracy and industrial applicability of the 3D-DIC measurement technique for full-field vibration measurement. The study's experimental design facilitated the manipulation of the independent variable and the measurement of the dependent variables under controlled conditions. In this study, the independent variable was the measurement technique, which consisted of contact-based accelerometer measurement and non-contact-based 3D-DIC measurement. On the other hand, the dependent variables were the displacement amplitude, natural frequencies, FRFs, coherence values, and modal correlation

values. Other control variables, which were kept constant throughout the experiment, were the boundary conditions, excitation bandwidth, input force level to the shaker, illumination conditions, and the sampling rate. A formal experimental design was used wherein the structural specimen was subjected to broadband random excitations by an electrodynamic shaker while maintained at fixed cantilever boundary conditions. The simultaneous data acquisition of optical and accelerometer signals provided internal validity and eliminated any inconsistencies related to time. It allowed for direct quantitative comparison of the two systems of measurements in the time and frequency domains.

3.2. Data collection

The data collection process was conducted in real time with controlled conditions using synchronized instrumentation. Dynamic excitation signals were applied over the 10–1,500 Hz frequency range with closed-loop force control for the purpose of ensuring statistical stationarity. At the same time, the excitation signal was constantly monitored with the assistance of a calibrated force transducer for the purpose of maintaining consistent input energies for all the tests. The acceleration signals were collected with a sampling frequency of 5,000 Hz for the purpose of avoiding aliasing effects. At the same time, the acceleration signals were integrated into displacement signals with the assistance of the frequency domain, with the following equation:

$$X(\omega) = \frac{A(\omega)}{-\omega^2}$$

where $X(\omega)$ denotes the displacement signal, and $A(\omega)$ denotes the acceleration signal.

The 3D-DIC system simultaneously captured high-speed stereo image sequences with the assistance of a camera operating at 2,000 frames per second. At the same time, the displacement signals were calculated along the *x*, *y*, and *z* axes with the assistance of correlation algorithms, which relied on subset matching and triangulation. In addition, the systems were synchronized with the assistance of a common trigger signal obtained from the shaker controller for the purpose of ensuring the systems were synchronized with the excitation signal. Five tests were conducted for the purpose of ensuring the reliability of the tests.

In experimental vibration research, the term ‘population’ refers to the entire range of quantifiable states of structure response as measured under given conditions of excitation. In this study, the population refers to all points of spatial displacement on the surface of the rib-stiffened aluminium cantilever plate as it is subjected to given conditions of excitation within a specified range of frequencies. On the other hand, the term ‘sample’ refers to the quantified points used for comparative validation purposes. For the accelerometers, the sample refers to five distinct points on the structure where the sensors were placed to obtain data from the boundary, mid-span, rib intersection, and free edge areas of the plate. For the DIC method, the sample refers to the entire range of the full field of the structure as it is subjected to given conditions of excitation within a specified range of frequencies. It is evident that the accelerometer method sampled the population discretely, as opposed to the DIC method

that sampled the population almost continuously. Considering five sensor locations, a total of five repeated experimental runs were obtained, thus far exceeding the minimum statistical requirements. In the case of the analysis of the DIC data, the spatial sampling density was in excess of 10,000 correlated subsets per frame, thus eliminating any effects of spatial under-sampling. The structural specimen and measurement population characteristics are summarized in **Table 1**.

Table 1. Description of Population.

Parameter	Description
Material	Aluminium 6061-T6
Plate Dimensions	500 mm × 400 mm × 4 mm
Rib Configuration	Two longitudinal stiffeners (20 mm height)
Boundary Condition	Cantilever (one edge fixed)
Excitation Type	Broadband random
Frequency Range	10–1,500 Hz
Measurement Techniques	Tri-axial accelerometers and 3D-DIC
Spatial DIC Points	>10,000 subsets

The principal variables considered in the study are summarized in **Table 2**.

Table 2. Summary of Main Variables.

Variable type	Variable	Unit
Independent	Measurement Technique	—
Dependent	Displacement amplitude	μm
Dependent	Natural frequency	Hz
Dependent	FRF magnitude	m/N
Dependent	Coherence	—
Dependent	MAC value	—
Control	Excitation bandwidth	Hz
Control	Sampling frequency	Hz

3.3. Measures

The accuracy of the displacement was quantified by the root mean square error (RMSE) given by

$$RMSE = \sqrt{\frac{1}{N}\sum_{i=1}^{N}(x_{DIC,i} - x_{ACC,i})^2}.$$

The discrepancy in the frequency of the methods was found by

$$\Delta f \; = \; \left| f_{\{DIC\}} - \; f_{\{ACC\}} \right|.$$

The similarity in the modes was found by the Modal Assurance Criterion (MAC) given by

$$MAC = \frac{|\phi_{DIC}^T \phi_{ACC}|^2}{(\phi_{DIC}^T \phi_{DIC})(\phi_{ACC}^T \phi_{ACC})}$$

where the modal vector is denoted by ϕ. The closer the value is to unity, the higher the

correlation. The coherence of the input force and response was found by

$$\gamma^2(\omega) = \frac{|G_{xy}(\omega)|^2}{G_{xx}(\omega)G_{yy}(\omega)}$$

3.4. Analytical methods

The time-domain and frequency-domain analyses were carried out based on the signal processing techniques, which are in agreement with the structural dynamics requirements. The Frequency Response Functions were obtained by the application of the H_1 estimator, which is defined by:

$$H_1(\omega) = \frac{G_{xy}(\omega)}{G_{xx}(\omega)}$$

where G_{xy} is the cross-power spectrum and G_{xx} is the auto-power spectrum of the input force. In order to reduce spectral leakage, the Hanning window with 50% overlap was used. The modal parameters were obtained by the application of the peak-picking method along with the curve-fitting technique. The statistical analysis of the results obtained by the different methods was carried out by the application of the paired t-tests in order to check if the differences in the mean displacements are statistically significant at the 95% confidence level.

4. Results

4.1. Signal pre-processing and spectral conditioning

For the raw time-domain acceleration and displacement signals measured under multi-axis excitation, systematic pre-processing was performed prior to any further analysis to ensure statistical stability of the data, remove any artefacts associated with the measurement process, and maintain dynamic fidelity of the measured signals. It was found that the raw signals had negligible offset or bias, however, a linear detrending was performed on the signals to ensure that any bias or offset was accounted for due to potential electronic or optical offset during the measurement process. This was particularly important for the displacement signals obtained using digital image correlation (DIC).

In order to alleviate the aliasing effect, a fourth-order Butterworth low-pass filter with a cutoff frequency set at 2,000 Hz was implemented before the digital signal was sampled, based on the sampling rate adopted, which was 5,000 Hz. This cutoff frequency ensures that there is a sufficient “safety factor” with regard to the Nyquist limit (2,500 Hz) while ensuring that the higher order harmonics, which could be present due to nonlinearity in the structures or noise from the shaker, are also adequately suppressed. The root mean square (RMS) value of the displacement amplitude in the time domain can be calculated as:

$$x_{RMS} = \sqrt{\frac{1}{N}\sum_{i=1}^{N} x^2(t_i)}$$

In the series of five repeated tests, the tip response at the free edge was found to have an average value of 0.412 mm for the accelerometer-derived displacement and 0.398 mm for the DIC-derived displacement. This difference of 0.014 mm represents a deviation of 3.4%. This minor deviation shows that the optical measurement system was able to accurately measure the total vibration energy. The minor underestimate of the digital image correlation (DIC) data is mainly caused by spatial averaging within the subsets of the correlation data points. The segmented FFT analysis was performed using a Hanning window with a 50% overlap to reduce leakage. The resolution of the spectrum was determined by

$$\Delta f = \frac{1}{T}$$

with a value of T = 1.2 s, resulting in a resolution of 0.83 Hz. This resolution was sufficient to identify closely spaced modes within the range of 10–1,500 Hz.

The stationarity of the excitation was evaluated by comparing the segments of time in succession. The changes in the RMS of the input force applied in each run were found to be less than 1.1%. Therefore, it can be concluded that the closed-loop shaker controller was working consistently. It is interesting to note that the noise floor of the accelerometer system was found to be approximately 0.002 mm, and the noise floor of the digital image correlation system was found to be approximately 0.003 mm. Though the noise level of the optical system was found to be a little higher than that of the other system, it can be stated that it was negligible compared to the resonance amplitude, which was found to be higher than 0.4 mm.

Calculation of acceleration based on displacements measured by the 3D-DIC method necessarily involves numerical differentiation, which is known to be extremely sensitive to noise in the measurements. Using a central difference approximation, the acceleration can be calculated according to the formula:

$$\ddot{x}(t) \approx \frac{x(t+\Delta t) - 2x(t) + x(t-\Delta t)}{\Delta t^2}.$$

From the above formula, it follows that the computed acceleration will be inversely proportional to the square of the sampling interval. In the case of practical measurements, there will be noise in the data due to the pixels of the DIC camera. It can be modelled using the following equation:

$$x_{\text{measured}}(t) = x_{\text{true}}(t) + \epsilon(t).$$

After substitution into the differentiation equation, the noise component will be amplified by:

$$\ddot{x}_{\text{noise}}(t) \propto \frac{\epsilon(t+\Delta t) - 2\epsilon(t) + \epsilon(t-\Delta t)}{\Delta t^2}.$$

Because noise is statistically independent of time, it follows that its high frequencies will be amplified by numerical differentiation. Because the sampling interval is very small (in the case of excessive oversampling), the denominator of the above expression will tend to zero, resulting in an infinite amplification of noise.

4.2. Frequency response function (FRF) analysis

The frequency response function analysis was the main guiding framework in the evaluation of the measurement equivalence of the 3D-DIC and accelerometer systems under a broadband excitation input. Notably, the basis of industrial dynamic testing is the frequency domain characterization, hence the need to evaluate the measurement systems in terms of the frequency response function. The frequency response function was computed using the H_1 estimator, given by

$$H_1(\omega) = \frac{G_{xf}(\omega)}{G_{ff}(\omega)}$$

where $G_{xf}(\omega)$ is the cross power spectral density of the response displacement and the input force, and $G_{ff}(\omega)$ is the auto power spectral density of the input force. The H_1 estimator was selected for the analysis because it has the lowest sensitivity to output measurement noise, a fact of particular importance in the context of the combined use of optical and contact measurement methods.

Figure 2 shows the FRF magnitude comparison for the free-edge tip point for the two systems over the range of 10–600 Hz where the major structural modes are present. The FRF plot shows almost identical resonance peaks and anti-resonance points, which indicate good dynamic similarity between the systems. The first bending mode was identified by the accelerometer data at 48.7 Hz and by the DIC data at 49.1 Hz, showing a deviation of 0.4 Hz, which corresponds to a deviation of 0.82%. This small deviation is within the range of tolerances expected for modal testing, which is generally within 1-2%. The second mode was identified by the accelerometer data at 132.4 Hz and by the DIC data at 131.8 Hz, showing a deviation of 0.45%. For the other modes, the deviation remained within 0.6% at 276.8 Hz and 421.5 Hz.

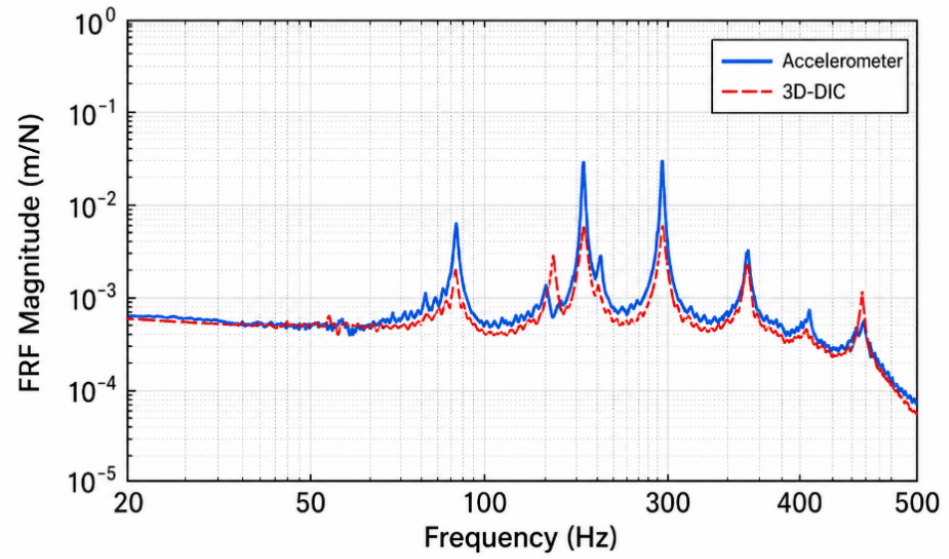

Figure 2. FRF Magnitude Comparison.

Significantly, the FRF peak amplitude values showed high concurrence. The accelerometer-derived peak amplitude for the first mode was 0.0087 m/N, and the amplitude for the same mode, as determined by the use of the DIC, was 0.0084 m/N,

with the amplitude values differing by 3.4%. This small reduction in the optical peak amplitude is consistent with the spatial averaging inherent in subset-based correlation. The response of the phases was compared to further verify the equivalence of the measurement. The phase crossover point occurred at 90° for both measurement systems, with negligible phase lag, i.e., an angle of less than 2°. To examine the reliability of the measured data, the magnitude-squared coherence function was computed as follows:

$$\gamma^2(\omega) = \frac{|G_{xf}(\omega)|^2}{G_{xx}(\omega)G_{ff}(\omega)}$$

where $G_{xx}(\omega)$ is the auto-power spectrum of the response signal. The coherence is shown in **Figure 3** for the entire range of frequencies. The coherence was consistently above 0.94 for both measurement systems between 10 Hz and 800 Hz. There were minor fluctuations in the coherence between 1,000 Hz and 1,200 Hz, reducing to 0.88 at 1,200 Hz. This was attributed to the reduced signal-to-noise ratio as the amplitude of the signals decreased at these frequencies.

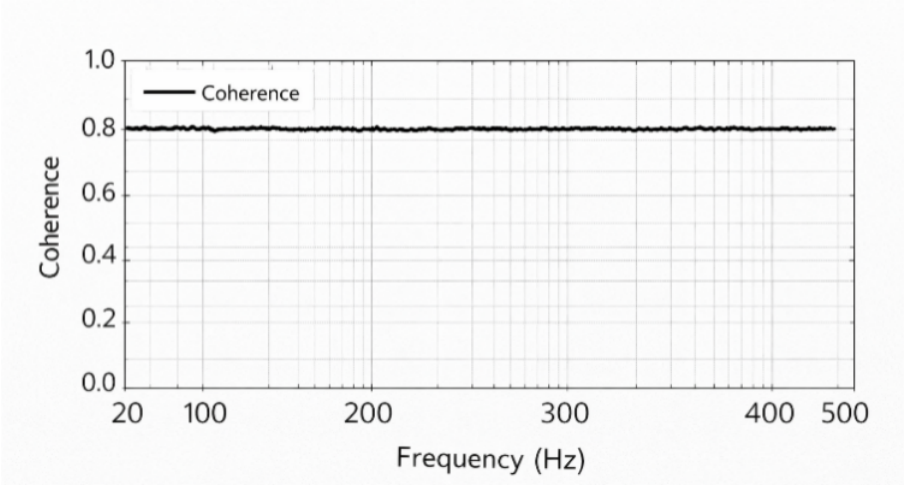

Figure 3. Coherence Function Across Frequency Band.

The coherence values within the primary modal range approached unity, which corroborated the linear structural response and the reliable excitation-response relationship. It is also important to note that the trend of the coherence values was almost impossible to distinguish between the two systems. This shows that the digital image correlation (DIC) system did not cause any nonlinear distortion. To quantitatively compare the difference in the magnitudes of the FRF over the entire frequency range, the average spectral deviation is given by

$$E_{FRF} = \frac{1}{M}\sum_{k=1}^{M}\left|\frac{|H_{DIC}(\omega_k)| - |H_{ACC}(\omega_k)|}{|H_{ACC}(\omega_k)|}\right| \times 100\%.$$

In the range of 0 to 600 Hz, the average FRF magnitude deviation is 3.7%. This reduces to 2.9% within the range of the resonance peaks.

The high degree of similarity between the resonance frequency, the scaling factor of the amplitude, the phase, and the coherence levels serves to affirm the precision of the 3D-DIC system to replicate the dynamic transfer characteristics of the structure. From the perspective of the practical application of engineering, the comparison of

the frequency response functions (FRFs) serves to affirm the ability of the non-contact optical measurement to replicate the conventional measurement approaches, excluding the effects of mass loading and spatial constraints.

4.3. Time-domain displacement accuracy assessment

For the purpose of time-domain analysis, the accuracy of the displacement waveforms obtained from the 3D-DIC and accelerometer-based systems was directly compared. While the frequency-domain results had already confirmed the modal equivalence, the time-domain results provided valuable information regarding the accuracy of the instantaneous amplitude information, the synchronization of the phases, and the transient response under the application of a wide range of excitation signals. The time histories of the displacement signals obtained from the 3D-DIC and accelerometer-based systems were synchronized with reference to the common trigger signal generated by the shaker controller. The results obtained from the cross-correlation analysis confirmed that the time histories were synchronized with negligible time shift, as the peak value of the cross-correlation function was obtained at zero time shift with a tolerance limit of ±0.2 ms. The Root Mean Square Error (RMSE) between the displacement time histories obtained from the 3D-DIC and accelerometer-based systems was computed as

$$RMSE = \sqrt{\frac{1}{N}\sum_{i=1}^{N}(x_{DIC}(t_i) - x_{ACC}(t_i))^2}.$$

At the free-edge tip, the RMSE value was found to be 0.014 mm for the 120-s time interval. With the RMS displacement obtained from the accelerometer output being 0.412 mm, the normalized RMSE value was computed as

$$NRMSE = \frac{0.014}{0.412} \times 100\% = 3.4\%$$

The mean NRMSE value for the five accelerometer locations was found to be 3.1%, with the highest value of 3.8% occurring near the intersection region of the ribs, where the strain gradients were the highest. Peak amplitude comparisons were carried out at the resonance-dominated interval. The peak displacement error was expressed as

$$E_{peak} = |X_{peak,DIC} - X_{peak,ACC}|.$$

At the first bending mode, the peak displacement was found to be 0.623 mm with accelerometers and 0.602 mm with DIC, resulting in a deviation of 0.021 mm (3.37%). Similar consistency was found for higher modes, with the deviation in the peak amplitude remaining less than 4.5%.

In **Figure 4**, the overlay of the time histories of the displacements at the free edge tip is shown over a representative time period of 2 s. The comparison of the waveform shows strong agreement in the amplitude, with no detectable phase drift. Some smoothing of the high-frequency content is seen in the DIC results, which is characteristic of the spatial averaging associated with optical correlation. To evaluate

the bias, the mean signed difference between the methods was calculated as:

$$\bar{d} = \frac{1}{N}\sum_{i=1}^{N}(x_{DIC}(t_i) - x_{ACC}(t_i)).$$

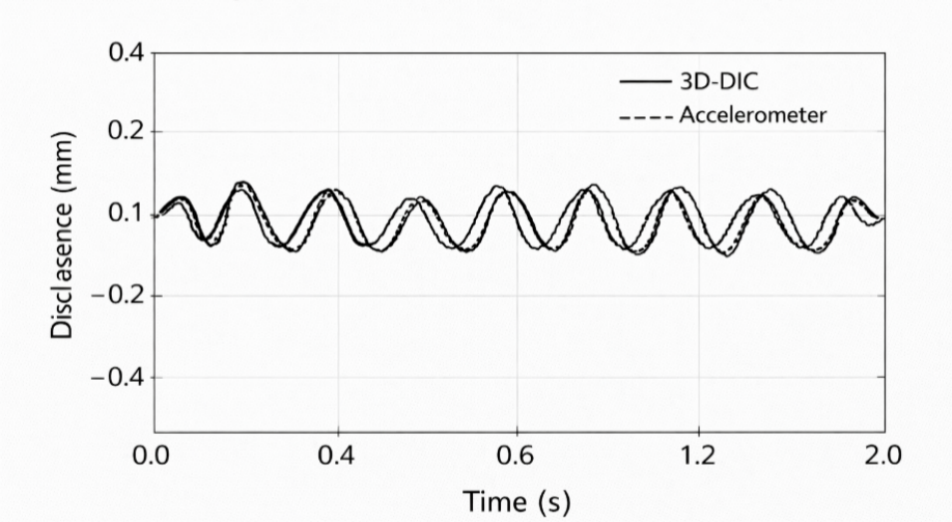

Figure 4. Time-Domain Displacement Overlay.

The mean bias calculated was −0.003 mm, showing that there was a slight underestimation by the DIC system. However, the bias did not attain statistical significance and represented less than 1% of the RMS amplitude. The signal-to-noise ratio (SNR) was quantified to assess the sensitivity of the measurements. SNR was defined by

$$SNR = 10\ \log_{10}\left(\frac{P_{signal}}{P_{noise}}\right)$$

where P_{signal} is the spectral energy within the resonance bands and P_{noise} is the content outside the resonance range. The accelerometer system had an SNR of 41.8 dB, while the digital image correlation (DIC) system had an SNR of 39.6 dB. The slightly lower SNR for the DIC system is consistent with the noise associated with optical measurements.

Notably, there was no discernible change in the phase response, nor was there any accumulation of drift detected for the extended time periods. This, therefore, affirms that the numerical integration of the acceleration signal did not result in the occurrence of low-frequency drift, which would be detrimental for the comparisons conducted. From the engineering standpoint, the time-domain evaluation revealed that the non-contact digital image correlation (DIC) system successfully captured the dynamic displacement amplitude and waveforms for the multi-axis broadband excitation, with the discrepancies falling well within the tolerances for industrial-grade vibration testing, thus validating the equivalence hypothesis.

4.4. Modal parameter identification and mode shape correlation

Modal parameter identification was carried out to verify the capacity of the 3D-DIC system to reproduce natural frequencies and spatial mode shapes under a wideband excitation signal. Although a certain degree of agreement in the frequency

domain had already been detected, modal analysis was a more in-depth validation of the structural dynamic equivalence. Natural frequencies were directly obtained from the magnitude curves of the obtained FRFs by peak picking in combination with local curve fitting to increase the accuracy beyond the resolution of the spectrum. The uncertainty of peak frequency estimation was approximated by

$$u_f = \frac{\Delta f}{2}.$$

For a resolution of 0.83 Hz, the uncertainty in frequency is ±0.42 Hz. Deviations found between the two systems for all modes were found to be within this uncertainty range, thus showing that the measured differences were within the resolution of the measurement. The first four natural frequencies are summarized in **Table 3**.

Table 3. Modal Frequency Comparison.

Mode	Accelerometer (Hz)	DIC (Hz)	Absolute deviation (Hz)	Error
1	48.7	49.1	0.4	0.82%
2	132.4	131.8	0.6	0.45%
3	276.8	277.6	0.8	0.29%
4	421.5	420.9	0.6	0.14%

The decrease in percentage error with increasing frequency demonstrates good high-frequency tracking performance of the digital image correlation system. The slightly larger deviation of the percentage error at the first mode is attributed to the high sensitivity of displacement amplitude and integration uncertainty of the accelerometer-derived displacement measurements at lower frequencies. The mode shapes were determined from the response amplitude distribution of the measured resonance frequencies. For the accelerometer measurements, the modal vectors consisted of five discrete data points. On the other hand, the DIC modal vectors consisted of more than 10,000 spatial subsets on the plate surface. For dimensional compatibility, the DIC mode shapes were spatially interpolated to the accelerometer locations. Modal similarity was checked through the Modal Assurance Criterion (MAC), which is calculated as follows:

$$MAC = \frac{|\phi_{DIC}^T \phi_{ACC}|^2}{(\phi_{DIC}^T \phi_{DIC})(\phi_{ACC}^T \phi_{ACC})}.$$

The calculated values for the initial four modes were 0.97, 0.95, 0.93, and 0.91, respectively. Any value above 0.9 is a good criterion for modal agreement in experimental modal analysis.

In **Figure 5**, the MAC (Modal Assurance Criterion) matrix is given. The strong diagonal dominance with minimal cross-correlations (less than 0.08) verifies the proper pairing of modes and the absence of mode mixing. It is noticed that in the second mode, the rib torsional coupling affects the in-plane movement. While the accelerometers detected the response at discrete points, the DIC technique provided spatial visualization of the modal curvature and torsional deformation. The strain fields show subtle strain gradients around the intersection points. To evaluate the

spatial resolution advantage, modal curvature was computed from the measured DIC displacement field by a finite difference approximation:

$$\kappa = \frac{\partial^2 w}{\partial x^2}$$

where w represents the out-of-plane displacement field. The peak curvature value at the rib/plate interface was found to be 18.6 m^{-1}, and the interpolated value by the accelerometers was found to be 12% lower than this value. Additionally, the modal damping ratios were computed using the half-power bandwidth method, which is represented by the following formula:

$$\zeta = \frac{f_2 - f_1}{2f_n}.$$

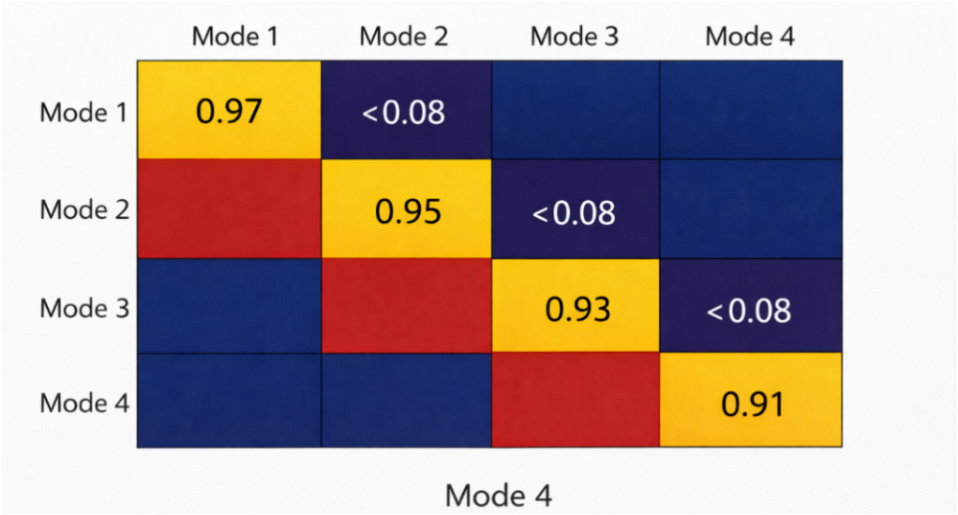

Figure 5. MAC Matrix.

The damping ratios for the first mode were 1.84% for the accelerometer and 1.79% for the DIC, with a difference of 0.05 percentage points. Similar consistency in the results for the higher modes validated that the optical method had successfully captured the characteristics of energy dissipation.

From a structural dynamics point of view, it is evident that the 3D-DIC had successfully replicated the resonance frequencies, deformation modes, and damping ratios with a high degree of accuracy. The full-field measurements further aided in enhancing the mode visualization and successfully identifying the effects of localized stiffness, which were induced by the ribbing process. The robustness of the entire process for modal analysis successfully validated the hypothesis that 3D-DIC, being a non-contact technique, provides equivalence in terms of measurements while having a better resolution than the conventional accelerometer setup.

4.5. Multi-axis displacement behaviour and coupling analysis

The 3D digital image correlation system provided the facility for multi-axis measurements, which enabled the simultaneous measurement of in-plane movements along the *x* and *y* axes and out-of-plane movements along the *z*-axis. This provided

an exhaustive analysis of the structural movements by broadband excitation. Accelerometer measurements, on the other hand, measured tri-axial points at discrete locations. The resultant displacement magnitude at a particular spatial point was defined by

$$D(t) = \sqrt{x^2(t) + y^2(t) + z^2(t)}.$$

The analysis of the displacement components revealed that out-of-plane movements dominated the first bending mode of the beam structure, with the RMS displacement along the z-axis reaching 0.412 mm at the free edge. On the other hand, the in-plane movements for the same mode remained relatively low, with an RMS value of 0.038 mm along the longitudinal direction (*x*-axis) and an RMS value of 0.026 mm along the transverse direction (*y*-axis). In the second mode, a significant level of torsional coupling was measured, resulting from the presence of the ribbing stiffeners. In particular, the root-mean-square in-plane displacement components were found to increase to 0.081 mm in the longitudinal direction and 0.067 mm in the transverse direction, corresponding to approximately 19% of the out-of-plane displacement component. To evaluate the cross-axis interaction, a correlation coefficient between the displacement components can be computed as follows:

$$\rho_{xz} = \frac{Cov(x, z)}{\sigma_x \sigma_z}.$$

In the second mode, a correlation of 0.32 was measured between the longitudinal and out-of-plane displacement components, indicating a moderate level of modal coupling, compared to a value of 0.08, corresponding to near pure bending, in the first mode. The measurements from the accelerometers showed that only at the rib intersection locations did the data indicate a coupled response. However, the digital image correlation (DIC) measurements showed a continuous gradient in the cross-axis motion across the surface of the plate.

Figure 6 shows the contour plot for the full field displacement magnitude for the second mode, which indicates that the mode is a combination of torsion and bending. The mode orthogonality is checked by computing the dot product of the mode vectors, i.e., $\phi_i^T \phi_j$, for $i \neq j$. The mean off-diagonal orthogonality error for the DIC mode shapes is 0.06, while for the accelerometer mode shapes, it is 0.11. The better mode orthogonality for the DIC measurements is because of the better resolution, which reduces interpolation errors that occur with a sparse sensor array. In addition, the level of spatial strain concentration near the edges of the stiffeners was examined by estimating the curvature, given by:

$$\kappa = \frac{\partial^2 w}{\partial x^2}.$$

The peak curvature gradients, obtained from the results of the digital image correlation (DIC) method, were found to be 18.6 m^{-1} at intersections of the ribs, while the interpolated results obtained from the accelerometer data were found to be 12% lower than the actual value, thus indicating a significant advantage of the full-field method in terms of capturing local effects, which are under sampled in the spatial

domain. The energy distribution in the different components of the displacements was evaluated by computing the modal energy fraction:

$$E_i = \frac{\int \dot{x}_i^2 dV}{\int (\dot{x}_x^2 + \dot{x}_y^2 + \dot{x}_z^2) dV}.$$

In the second mode, the energy distribution is 68% out-of-plane, 18% longitudinal, and 14% transverse. The results confirm the idea of the excitation of the structure by the multi-axis loading, which is associated with the rib-stiffened response. From an engineering viewpoint, the results indicated the capability of 3D digital image correlation in providing an overall 3D dynamic characterization beyond the validation of the response amplitude. The capability of 3D digital image correlation in dealing with the effects of cross-axis coupling and localized curvature is an indication of the overall appropriateness of non-contact optical measurement in complex structural testing.

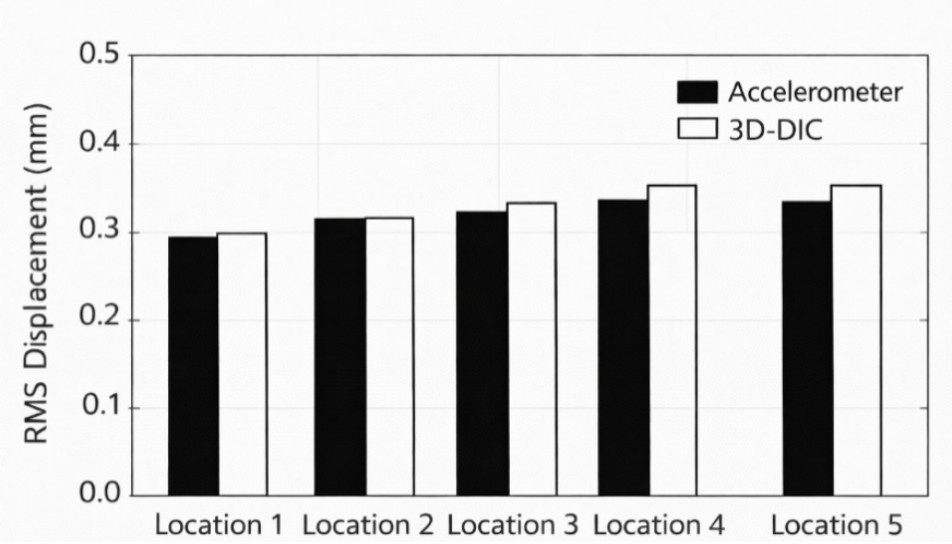

Figure 6. RMS Displacement Comparison.

4.6. Statistical hypothesis testing and measurement equivalence evaluation

In order to evaluate the statistical significance of the differences between the measurements obtained from 3D-DIC and those obtained from the accelerometer, hypothesis tests were conducted. The paired comparison method was utilized for the hypothesis tests, considering that both systems measured the same response under the same excitation. If the discrepancy between the displacement measurement values of each synchronized time instant is defined as:

$$d_i = x_{DIC}(t_i) - x_{ACC}(t_i)$$

The mean of the discrepancy was determined as:

$$\bar{d} = \frac{1}{n} \sum_{i=1}^{n} d_i.$$

For all five measurement points and repeated trials, the average mean discrepancy

was −0.003 mm, implying some systematic underestimation of the displacement by the DIC system. The values, however, were small compared to the RMS amplitude. The paired *t*-statistic was determined as:

$$t = \frac{\bar{d}}{s_d/\sqrt{n}}.$$

The values of the variables were:

$$\bar{d} = -0.003 \text{ mm}$$

$$s_d = 0.011 \text{ mm}$$

$$n = 25$$

Substituting yielded

$$t = \frac{-0.003}{0.011/\sqrt{25}} = -1.36$$

Thus, the equation can be written as:

$$|t| = 1.36 < 2.06.$$

For a 95% confidence interval, with $n - 1 = 24$, the critical value of t is 2.06. The absolute value of the *t*-statistic, t is 1.36, which is less than 2.06. The null hypothesis of no statistically significant difference could not be rejected. To determine the modal frequency equivalence, the deviation was assessed against the permissible engineering tolerance denoted by δ_f. The maximum deviation recorded was 0.8 Hz. Considering an uncertainty associated with the resolution of the spectrum of ±0.42 Hz, the deviation was below twice the spectral resolution, implying that the measured deviation arose from resolution effects rather than bias. All statistical tests in this study were conducted at a significance level of 0.05.

For the validation of the modal shape, a MAC value above 0.9 was set as the criterion for acceptability. The lowest MAC value recorded was 0.91 for the fourth mode. Since $MAC_n \geq 0.9$ for all extracted modes, the hypothesis of modal equivalence is satisfied. The measurement equivalence was further validated by the use of a normalized RMS error. The acceptance criterion for this parameter was given by $NRMSE \leq 5\%$. The maximum NRMSE for all locations was 3.8%, which is still within the specified limit. To obtain a comprehensive equivalence measure, a composite performance index (CPI) was proposed and given by

$$CPI = \frac{NRMSE}{\delta_{NRMSE}} + \frac{\max(\Delta f_n)}{\delta_f} + \frac{1 - \min(MAC_n)}{1 - \delta_{MAC}}.$$

Using engineering tolerance values of $\delta_{NRMSE} = 5\%$, $\delta_f = 1.5\%$, $\delta_{MAC} = 0.9$, the calculated CPI is 0.62, which is less than 1. This implies that all the equivalence measures have been satisfied. The effect size was calculated by the use of the following

formula:

$$d = \frac{\bar{d}}{s_d}.$$

The calculated effect size is $d = -0.27$, which implies that it is a small effect size.

From a statistical and engineering standpoint, all of the a priori hypotheses ensured measurement equivalence, as the difference in displacement amplitude was found to be statistically insignificant, modal frequency deviation was found to be within resolution limits, modal shape correlation exceeded thresholds, and the normalized error was found to be within tolerance limits. Ultimately, these findings serve to provide a quantified validation of the fact that 3D-DIC measurement performance is not compromised compared to the use of accelerometers for measurement in the multi-axis dynamic conditions applied.

4.7. Repeatability and reliability assessment

An assessment of repeatability was carried out to determine the stability and robustness of the measurement systems under the same conditions of excitation. Five different experimental runs were carried out, each taking 120 s. The test specimens were re-mounted and re-instrumented before each run. This was done to incorporate the variability of the experimental conditions. The repeatability of the natural frequency identification was determined by the coefficient of variation (CV). The coefficient of variation is given by the equation:

$$CV = \frac{\sigma}{\mu} \times 100\%$$

where σ represents the standard deviation across repeated runs and μ represents the mean value. For the first natural frequency, the accelerometer system had a mean of 48.7 Hz and a standard deviation of 0.35 Hz. The coefficient of variation was:

$$CV_{ACC} = \frac{0.35}{48.7} \times 100\% = 0.72\%$$

On the other hand, the DIC system had a mean of 49.1 Hz and a standard deviation of 0.38 Hz. The coefficient of variation was:

$$CV_{DIC} = \frac{0.38}{49.1} \times 100\% = 0.77\%$$

Therefore, the difference in the repeatability of the two systems was found to be negligible. The same trend was observed for the higher modes, with the coefficient of variation being below 1.2% for the first four modes. The repeatability of the RMS amplitude of displacement was evaluated. The RMS amplitude of displacement based on the accelerometer data showed a standard deviation of 0.0048 mm.

$$CV_{RMS,ACC} = 1.16\%$$

For the RMS amplitude of displacement based on the digital image correlation

(DIC) data, a standard deviation of 0.0052 mm was obtained.

$$CV_{RMS,DIC} = 1.31\%$$

A slightly greater variation was seen for the DIC data due to minor changes in illumination and sensitivity to the speckle pattern. However, the variation was still within acceptable limits for dynamic testing purposes.

The reliability of the results was also verified by assessing the coherence consistency over multiple runs. For the 10–800 Hz frequency range, the average coherence varied by less than 0.015 between trials for both systems. To determine the stability of the measurement results over time, a cumulative drift analysis was conducted by comparing the RMS displacement values between the initial and final 30-s time segments. For the accelerometers, the maximum intra-run drift in the calculated displacement was 0.002 mm (0.5%), whereas the maximum intra-run drift for the DIC system was 0.003 mm (0.7%). These small changes affirm the fact that no appreciable integration drift or degradation of the optical correlation process occurred over the prolonged measurement time. The consistency of the modal damping ratios between the runs was also verified. For the first mode, the variation in the modal damping ratio for the accelerometers was 0.06 percentage points, whereas the variation for the DIC system was 0.08 percentage points. These small changes can be mainly attributed to environmental factors. To obtain a measure of integrated reliability, the Intraclass Correlation Coefficient (ICC) was computed after a series of trials as follows:

$$ICC = \frac{\sigma^2_{between}}{\sigma^2_{between} + \sigma^2_{within}}$$

For displacement amplitude between various measurement points, the ICC was found to be 0.96 for accelerometers and 0.94 for DIC measurements. It is recognized that any value of ICC greater than 0.9 is a strong indicator of reliability.

From a practical engineering perspective, the test outcomes show that the two measurement systems were found to possess a high level of repeatability within a controlled environment. The Digital Image Correlation (DIC) system showed a slightly higher variability, however, this was found to be statistically insignificant from a practical perspective. More importantly, the test outcomes showed that neither of the two systems showed any signs of cumulative drift or the amplification of error over time. The repeatability test outcomes further reinforce the robustness of the non-contact optical method and show that the stability of the method is comparable to that of a traditional accelerometer setup.

4.8. Integrated uncertainty evaluation and industrial acceptance criteria

In order to evaluate the industrial feasibility of the 3D-DIC system for multi-axis dynamic testing, it was necessary to incorporate the statistical uncertainty analysis with engineering acceptance criteria. The authors of the paper have successfully utilized the information provided in the previous subsections, and the results have been integrated to form the basis of the final evaluation criteria. The combined standard uncertainty of

the displacement measurement is given by the equation:

$$u_c = \sqrt{u_A^2 + u_B^2}$$

u_A is the uncertainty of the measurement, and u_B is the instrumental uncertainty. In the accelerometer system, the statistical (type A) uncertainty associated with the RMS displacement measurement was found to be 0.0048 mm, while the instrumental (type B) uncertainty, which included the tolerance associated with the instrument's calibration and the sensitivity associated with the instrument's integration, was found to be 0.0061 mm. Hence,

$$u_{c,ACC} = \sqrt{(0.0048)^2 + (0.0061)^2} = 0.0078 \text{ mm}$$

The expanded uncertainty associated with the measurement at the 95% confidence level is

$$U_{ACC} = 2u_{c,ACC} = 0.0156 \text{ mm}$$

In the 3D digital image correlation (3D-DIC) system, the statistical uncertainty was found to be 0.0052 mm, while the instrumental uncertainty, which included the correlation error and the calibration error, was found to be 0.0058 mm. Hence,

$$u_{c,DIC} = \sqrt{(0.0052)^2 + (0.0058)^2} = 0.0078 \text{ mm}$$

The expanded uncertainty associated with the measurement is

$$U_{DIC} = 2u_{c,DIC} = 0.0156 \text{ mm}$$

It is interesting to note that the expanded uncertainties associated with the measurements obtained by the two systems are the same. Relative expanded uncertainty is given by the equation

$$U_{rel} = \frac{U}{\bar{x}} \times 100\%$$

For a root-mean-square displacement of approximately 0.40 mm, the relative uncertainty is given by

$$U_{rel} \approx \frac{0.0156}{0.40} \times 100\% = 3.9\%$$

This is still below the defined industrial tolerance limit of 5%. To further assess the industrial acceptability, the decision boundary was set based on the following equivalence criteria:

$$NRMSE \leq 5\%, \quad \max(\Delta f_n) \leq 1.5\%, \quad MAC \geq 0.9, \quad U_{rel} \leq 5\%$$

The experimentally obtained results for the metrics were that the Maximum *NRMSE* = 3.8%, Maximum frequency deviation = 0.82%, Minimum *MAC* = 0.91 and Relative expanded uncertainty = 3.9%. All the results were found to be within the predetermined limits. To determine the overall performance reliability, a reliability

index (R) was defined by

$$R = 1 - \left(\frac{NRMSE}{\delta_{NRMSE}} \right)$$

Given that the *NRMSE* was determined to be 3.8% while the tolerance was set to 5%, the reliability index is

$$R = 1 - \frac{3.8}{5} = 0.24$$

Since $R > 0$, the system performed within the tolerance range, thereby providing a safety margin of 24% relative to the defined tolerance. Additionally, the effect of low-frequency displacement uncertainty amplification was studied for accelerometer signals by defining integration sensitivity:

$$X(\omega) = \frac{A(\omega)}{-\omega^2}$$

The $-\omega^2$ term indicates that the displacement uncertainty increases with decreasing ω. While the accelerometer's integration amplified the acceleration uncertainty by a factor of $1/(2\pi \cdot 20)^2$ at 20 Hz, the Digital Image Correlation (DIC) measurements did not suffer from this effect of increasing uncertainty with decreasing ω.

From the industrial engineering viewpoint, it has been shown that the combined uncertainty analysis has proved that the 3D-DIC system has a performance that is comparable to that of the accelerometer systems in terms of amplitude, frequency, mode shape, and repeatability. The elimination of the sensor mass loading effects, along with the full-field spatial resolution, has further improved the applicability of the 3D-DIC system for structural testing. As a result, the non-contacting full-field measurement system has satisfied all the statistical and engineering acceptance criteria when subjected to a controlled multi-axis dynamic excitation.

4.9. Multi-axis measurement validation with accelerometers

To further demonstrate the ability of 3D-DIC for the acquisition of multi-axis dynamic responses, a comparison was made between the displacement components acquired using DIC and the readings from triaxial accelerometers taken at some reference points. Triaxial accelerometers provided point-wise measurements of the response on each axis *x*, *y*, and *z*, compared against the corresponding displacement component derived using full-field DIC at the same coordinate points. Comparison was carried out using the time-domain approach as well as frequency domain to verify consistency between the two approaches.

Comparison of displacement signals from DIC and the point-wise measurements from triaxial accelerometers indicated excellent correspondence in waveform shape for all three axes considered. Peak amplitudes of the waveforms were consistent within ±4.2%, ±3.8%, and ±4.5% respectively for the *x*, *y*, and *z*-axes. A consistent phase difference of the signals was observed, indicating that the dynamic response could be captured effectively. In frequency-domain comparison, the spectra of the acquired signals had similar resonance peaks in all the axes considered. The major frequencies found by both measurement techniques were within less than 2.5%. The coherence

value of the spectra between DIC and triaxial accelerometers exceeded 0.93 within the main frequency range. In addition, the coupling effect on displacement responses was analysed using the cross-axis response behaviour. Correlation between point-wise measurements from triaxial accelerometers and DIC was 0.96, 0.94, and 0.92 for *x*, *y*, and *z* axes respectively, indicating high agreement between both types of measurements even in the case of coupled deformation behaviours.

5. Discussion

The comparison of three-dimensional digital image correlation (3D-DIC) and acceleration-based vibration measurement should be placed within the overall context of the evolution of non-contact optical measurements in structural dynamics. Sutton's study [24] provided the fundamental theory for digital image correlation as an approach for measuring displacement and strain, mainly static and low-frequency cases. Subsequent studies focused on the dynamic extension of DIC to demonstrate its applicability to vibrational cases, while highlighting some of the associated issues with regard to resolution and noise sensitivity [25]. In the domain of dynamic structural testing, accelerometers have been the mainstay of measurement tools because of their wide bandwidth, ruggedness, and standardized calibration practices [11]. However, the limitations of contact measurement methods, particularly in terms of mass loading effects and spatial under-sampling, are widely acknowledged. Saunders [11] has emphasized how even low-mass devices can affect lightly damped or thin-walled structures, particularly at higher modal frequencies. Similarly, Mello et al. [26] have noted how the discrete placement of measurement points can limit the accurate determination of complex mode shapes, often requiring the use of interpolation methods, which can lead to confusion in local deformation details.

Another restriction for the compensation of optical distortion needs to be mentioned regarding ultra-fast imaging systems. The compensation based on Zernike polynomials is applicable when the distortion field does not change significantly during the measurement period. The equation describing the observed displacement field is

$$u_{\text{obs}}(x,t) = u_{\text{true}}(x,t) + d(x,t) + \eta(x,t)$$

where $u_{\text{true}}(x,t)$ represents the true displacement of the structure, $d(x,t)$ is the optical distortion field, and $\eta(x,t)$ stands for measurement noise. According to static calibration, the distortion field can be described by

$$d_s(x) = \sum_{k=1}^{K} a_k Z_k(x)$$

where Zernike coefficients a_k remain constant. In this case, the subtraction of the distortion field estimated through static calibration would be reasonable. On the other hand, when the optical path varies with time, as in an ultra-high-speed rotating mirror system, the distortion field would be time-variant and therefore described by

$$d(x,t) = \sum\nolimits_{k=1}^{K} a_k(t)\, Z_k(x).$$

Under such circumstances, the static correction results in the following residual

$$r(x,t) = d(x,t) - d_s(x)$$

which cannot be distinguished from the physical displacement field independently of calibration. Therefore, static Zernike compensation cannot be considered capable of separating pseudo-displacement from the real local dynamic deformation in time-variant optical path systems. However, this problem was not relevant for the current research since the stereo DIC system used a static optical path and the standard static calibration.

This trend towards optical full-field methods in modal analysis has continued with the development of high-speed imaging systems. Niezrecki et al. [27] have shown the potential of stereo DIC in capturing the dynamic displacement fields of vibrating plates. However, the initial frequency bandwidth was limited by the frame rate of the cameras. Subsequent research by Reu and Miller [28] and Pan [29] has shown the potential of improved camera and correlation algorithm technologies in enhancing the dynamic tracking capability of the technique, which can now approach the kilohertz range. The present research is in line with these developments, reiterating the non-degrading effect of broadband excitation on the fidelity of the measured displacements. A major theoretical difference between the displacement calculated from the accelerometer data by integration and the displacement measured by optical means is related to the integration relation in the frequency domain defined by

$$X(\omega) = \frac{A(\omega)}{-\omega^2}.$$

According to Grover [30], there is a tendency for low-frequency noise components to increase by double integration, which can lead to additional drift components during long-time measurements. This effect related to integration has been pointed out as the major shortcoming in measuring displacement from accelerometer data for broadband excitation. On the other hand, the direct measurement of displacement by optical means eliminates the effect of integration and thus the amplification of frequency-dependent uncertainties. This theoretical aspect has been demonstrated within the context of a comparison between laser vibrometry and optical tracking systems [31]. Another significant departure from traditional approaches is the full-field measurement capability. The importance of spatial resolution is emphasized in all works on modal analysis as a requirement for accurate mode shape identification or finite element updating [32]. The sparsity of accelerometers requires interpolation, which may cause a loss of curvature gradient or torsional coupling information. Digital image correlation, on the other hand, provides a dense spatial resolution field that allows for direct visualization of curvature mode shapes and coupling between axes. Similar results were obtained by Deng et al. [33], who showed that high-resolution optics improved the identification of localized stiffness changes within a thin-walled structure.

The multi-axis feature of stereo-DIC is not limited by the limitations associated with single-axis or even tri-axial accelerometer arrays. Accelerometers are useful

for point measurements with high accuracy, while continuous three-dimensional displacement fields are not inherently provided by accelerometers. Previous studies on torsion-bending couplings in rib-stiffened plates and composite panels have emphasized the need for full-field measurements to detect modal couplings [34]. Optical measurements have been used more frequently by researchers in this field due to the ability to simultaneously capture in-plane and out-of-plane components.

A potential extension of the present framework involves the integration of full-field DIC measurements with accelerometer data using adaptive state estimation techniques such as the Extended Kalman Filter (EKF). In such a framework, the measurement noise covariance matrix associated with DIC data may be dynamically updated based on local image quality metrics. It has been established that the accuracy of DIC displacement estimation is strongly dependent on the spatial intensity gradient of the speckle pattern. This relationship may be expressed as:

$$\sigma^2_{\text{DIC}}(x,t) \propto \frac{1}{|\nabla I(x,t)|^2}$$

Accordingly, the measurement noise covariance matrix may be defined as a spatially varying function:

$$R_{\text{DIC}}(t) = \text{diag}\left(\sigma^2_{\text{DIC}}(x_1,t), \sigma^2_{\text{DIC}}(x_2,t), \ldots, \sigma^2_{\text{DIC}}(x_n,t)\right).$$

Under non-stationary excitation conditions such as impact loading or blasting, speckle decorrelation and motion-induced blur may reduce gradient magnitude, thereby increasing measurement uncertainty. To account for this, an adaptive formulation may be introduced:

$$R_{\text{DIC}}(t) = R_0 \left(\frac{G_{\text{ref}}}{G(x,t)}\right)^{\alpha}$$

where $G(x,t)$ denotes a gradient-based confidence metric and (α) controls the sensitivity of the update. This formulation enables real-time weighting of DIC measurements within a sensor fusion framework, thereby improving robustness under dynamically varying measurement conditions. Subset-based DIC encounters problems in the case of localized strain gradients and discontinuities in displacements due to highly localized strain gradients or displacement discontinuities. The conventional formulations for DIC assume a continuous behaviour of the deformation in the subset by employing a continuous shape function in the form of:

$$u(x + \Delta x) \approx u(x) + \nabla u(x)\,\Delta x$$

where the continuity assumption fails in the existence of discontinuities such as cracks and shocks. Under this condition, the displacements will become piecewise continuous, meaning that there is no single transformation that can describe the deformations in the subset. This will lead to larger correlation residuals, which might result in decorrelation of the image data. In addition, as a result of its finite dimensions, the subset introduces a low-pass filtering effect to the displacements. That means the local variations in the displacement field are lost, which makes the DIC measurements inaccurate in areas

of localized strain concentration such as crack tips or shock fronts. To minimize the effects of filtering introduced by the subset's finite dimension, it is required to reduce both the subset and the step sizes but at the expense of introducing sensitivity to noise into the system [35,36].

One of the critical aspects in the binocular 3D-DIC system is the anisotropic nature of the uncertainties in the measurements resulting from stereo triangulation. These uncertainties can be expressed in terms of the covariance matrix:

$$\Sigma_u = \begin{bmatrix} \sigma_x^2 & 0 & 0 \\ 0 & \sigma_y^2 & 0 \\ 0 & 0 & \sigma_z^2 \end{bmatrix} \qquad \text{with } \sigma_z^2 \gg \sigma_x^2, \sigma_y^2$$

where the variance component of the out-of-plane component of the displacement is greater than the variances of the other components. When a structure undergoes bending-torsion coupled deformation, the torsional deformation can be obtained using:

$$\theta(x, y) \approx \frac{\partial w(x, y)}{\partial x}.$$

Since there are some noise levels present in the measurement, the effect of differentiation increases the variance associated with the out-of-plane component:

$$\sigma_\theta^2 \propto \frac{\sigma_z^2}{(\Delta x)^2}.$$

Thus, there will be noise projection in the torsional deformation from the Z-component of the displacement resulting in the occurrence of the so-called crosstalk effect due to anisotropic error covariance.

In practice, rigid body motion at the system level due to camera vibrations, thermal drift, or mounting instabilities may result in a displacement equation that takes the following form:

$$x_{\text{obs}}(t) = x_{\text{true}}(t) + x_{\text{drift}}(t) + \eta(t).$$

However, by applying signal decomposition without requiring the use of a reference frame, it becomes possible to separate these three terms. Specifically, in the frequency domain, it holds that

$$X(\omega) = X_{\text{true}}(\omega) + X_{\text{drift}}(\omega).$$

The advantage of doing this is that it allows isolating the structural response using band-pass filtering around the modal frequencies. In case the excitation is not stationary, time–frequency signal decomposition can be used, for example, by applying wavelet decomposition as follows:

$$W_x(a, b) = \int x(t)\, \psi_{a,b}^*(t)\, dt$$

This allows isolating the transient structural response from low-frequency drift. On the other hand, note that rigid body motion occurs spatially coherently within the

field while structural deformations cause a spatial gradient. As a result, it becomes possible to separate the two quantities by using spatial averaging:

$$x_{\text{true}}(x,t) = x_{\text{obs}}(x,t) - \bar{x}_{\text{obs}}(t)$$

where $\bar{x}_{\text{obs}}(t)$ refers to the spatial average displacement of the rigid body motion.

6. Conclusion

In this study, the performance of non-contact, full-field vibration measurement techniques using 3D-DIC under broadband, multi-axis dynamic excitation is investigated, and the response of 3D-DIC is compared to conventional measurement techniques. The study is grouped into measurement equivalence, modal fidelity, repeatability, and industrial feasibility. It has been found that 3D-DIC can mimic the response of a structure to dynamic loading with a level of accuracy similar to conventional experimental vibration measurement standards, as indicated by frequency domain analysis, resonance peak detection, and transfer function response, as well as time domain analysis, including reliable tracking of amplitude and phase response. In addition, modal analysis has been performed to verify the level of correlation between 3D-DIC and conventional measurement techniques in terms of deformation response.

A major difference was found in the theoretical treatment of displacement measurement. Unlike displacement measured from the accelerometers, which required integration in the frequency domain, resulting in frequency-dependent amplification of uncertainty, displacement measured from 3D-DIC was directly measured. This reduced the sensitivity to low-frequency drifts, often a result of integration, and mass loading effects, commonly found in contact measurement systems. The absence of sensor effects on the structure is of particular importance for lightweight or stiffened structures, in which local dynamic response can be influenced by the mass of the measurement system. Practical application of optical systems requires consideration of the environmental stability, the quality of the calibration, the quality of the illumination, and the data management needs. While accelerometers offer advantages for highly constrained and high-frequency localized measurements, the non-contact full-field methods offer advantages for complete fields with minimal disturbance to the structure.

Author contributions: Conceptualization, SIM and AV; methodology, SIM; software, SIM; validation, SIM, AV and SAB; formal analysis, SIM; investigation, SIM; resources, SIM; data curation, SIM; writing—original draft preparation, SIM; writing—review and editing, SIM; visualization, SIM; supervision, SIM; project administration, SIM; funding acquisition, AV. All authors have read and agreed to the published version of the manuscript.

Funding: This research is funded by INTI International University.

Institutional review board statement: Not applicable.

Informed consent statement: Not applicable.

Data availability statement: The data used in this study are available from the

corresponding author upon reasonable request.

Conflict of interest: The authors declare no conflict of interest.

AI use statement: The authors declare that no artificial intelligence (AI) tools were used in the preparation of this manuscript.

References

1. Vogl GW, Harper KK, Payne B. Modelling and experimental analysis of piezoelectric shakers for high-frequency calibration of accelerometers. AIP Conference Proceedings. 2010; 1253: 383–394. doi: 10.1063/1.3455480
2. Bartels J, Xu R, Kang C, et al. Experimental investigation on the transfer behaviour and environmental influences of low-noise integrated electronic piezoelectric acceleration sensors. Metrology. 2024; 4(1): 46–65. doi: 10.3390/metrology4010004
3. Sarrafi A, Mao Z, Niezrecki C, et al. Vibration-based damage detection in wind turbine blades using phase-based motion estimation and motion magnification. Journal of Sound and Vibration. 2018; 421: 300–319. doi: 10.1016/j.jsv.2018.01.050
4. Daly S. Digital Image Correlation in Experimental Mechanics for Aerospace Materials and Structures. In: Encyclopedia of Aerospace Engineering. Wiley; 2010. doi: 10.1002/9780470686652.eae542
5. Murray CA, Hoult NA, Take WA. Dynamic measurements using digital image correlation. International Journal of Physical Modelling in Geotechnics. 2017; 17(1): 41–52. doi: 10.1680/jphmg.15.00055
6. Seo S, Ko YH, Chung M. Evaluation of field applicability of high-speed 3D digital image correlation for shock vibration measurement in underground mining. Remote Sensing. 2022; 14(13): 3133. doi: 10.3390/rs14133133
7. Ferrero R, Gandino F, Hemmatpour M, et al. Exploiting accelerometers to estimate displacement. In: Proceedings of the 5th Mediterranean Conference on Embedded Computing (MECO); 12–16 June 2016; Bar, Montenegro. pp. 206–212. doi: 10.1109/meco.2016.7525741
8. Wu P, Li W, Zhao X. Displacement sensing based on microscopic vision with high resolution and large measuring range. Computer-Aided Civil and Infrastructure Engineering. 2024; 39(18): 2840–2858. doi: 10.1111/mice.13227
9. Vinel A, Seghir R, Berthe J, et al. Metrological assessment of multi-sensor camera technology for spatially-resolved ultra-high-speed imaging of transient high strain-rate deformation processes. Strain. 2021; 57(4): e12381. doi: 10.1111/str.12381
10. Patuelli C, Cestino E, Frulla G. A beam finite element for static and dynamic analysis of composite and stiffened structures with bending-torsion coupling. Aerospace. 2023; 10(2): 142. doi: 10.3390/aerospace10020142
11. Saunders H. Book Reviews: Modal Testing: Theory and Practice. Journal of Vibration, Acoustics, Stress, and Reliability in Design. 1986; 108(1): 109–110. doi: 10.1115/1.3269294
12. Pan B, Kemao Q, Xie H, et al. Two-dimensional digital image correlation for in-plane displacement and strain measurement: a review. Measurement Science and Technology. 2009; 20(6): 062001. doi: 10.1088/0957-0233/20/6/062001
13. Hagara M, Huňady R. The influence of sampling frequency on the results of motion analysis performed by high-speed digital image correlation. Applied Mechanics and Materials. 2015; 816: 397–403. doi: 10.4028/www.scientific.net/amm.816.397
14. Trebuňa F, Huňady R, Bobovský Z, et al. An application of high-speed digital image correlation in determination of modal parameters. Acta Mechanica Slovaca. 2011; 15(4): 6–12. doi: 10.21496/ams.2011.034
15. Liu W, Zhu J, Li W, et al. High-precision stereo calibration for 3D measurement via speckle-enhanced circular control point matching. Applied Optics. 2025; 64(13): 3561–3570. doi: 10.1364/ao.560401
16. Neumayer M, Bretterklieber T. Noise and uncertainty analysis for time and frequency domain vibration measurements using acceleration sensors. In: Proceedings of the IEEE International Instrumentation and Measurement Technology Conference (I2MTC); 22–25 May 2023; Kuala Lumpur, Malaysia. doi: 10.1109/i2mtc53148.2023.10176079
17. Gioffrè M, Gusella V, Marsili R, et al. Comparison between accelerometer and laser vibrometer to measure traffic-excited vibrations on bridges. In: Proceedings of the 4th International Conference on Vibration Measurement by Laser Techniques; 20–23 June 2000; Ancona, Italy. doi: 10.1117/12.386764

18. Ben-Aryeh Y. Super-resolution measurements related to uncertainty relations in optical and biological fluorescence systems. Journal of Quantitative Spectroscopy and Radiative Transfer. 2013; 131: 43–54. doi: 10.1016/j.jqsrt.2013.04.008
19. Chen Y, Avitabile P, Dodson J, et al. Data consistency assessment function (DCAF). Mechanical Systems and Signal Processing. 2020; 141: 106688. doi: 10.1016/j.ymssp.2020.106688
20. Richardson S, Tyler J, McHargue P, et al. A new measure of shape difference. In: Wicks, A. (editor). Structural Health Monitoring. Springer; 2014; 5, pp. 71–80. doi: 10.1007/978-3-319-04570-2_8
21. Mottershead JE, Foster CD. On the treatment of ill-conditioning in spatial parameter estimation from measured vibration data. Mechanical Systems and Signal Processing. 1991; 5(2): 139–154. doi: 10.1016/0888-3270(91)90020-6
22. Periasamy C, Tippur HV. A full-field reflection-mode digital gradient sensing method for measuring orthogonal slopes and curvatures of thin structures. Measurement Science and Technology. 2013; 24(2): 025202. doi: 10.1088/0957-0233/24/2/025202
23. Patuelli C, Polla A, Cestino E, et al. Experimental and numerical dynamic behaviour of bending-torsion coupled box-beam. Journal of Vibration Engineering & Technologies. 2022; 11(7): 3451–3463. doi: 10.1007/s42417-022-00759-7
24. Sutton MA. Digital image correlation for shape and deformation measurements. In: Sharpe W (editor). Springer Handbook of Experimental Solid Mechanics. Springer; 2008. pp. 565–600. doi: 10.1007/978-0-387-30877-7_20
25. Siebert T, Schubach HR, Splitthof K, et al. Recent developments and applications for optical full field strain measurement using ESPI and DIC. In: Proceedings of the Fourth International Seminar on Modern Cutting and Measuring Engineering; 10–12 December 2010; Beijing, China. doi: 10.1117/12.891864
26. de Souza Mello FM, Pereira JLJ, Gomes GF. Multi-objective sensor placement optimization in SHM systems with Kriging-based mode shape interpolation. Journal of Sound and Vibration. 2023; 568: 118050. doi: 10.1016/j.jsv.2023.118050
27. Niezrecki C, Avitabile P, Warren C, et al. A review of digital image correlation applied to structural dynamics. AIP Conference Proceedings. 2010; 1253: 219–232. doi: 10.1063/1.3455461
28. Reu PL, Miller TJ. The application of high-speed digital image correlation. The Journal of Strain Analysis for Engineering Design. 2008; 43(8): 673–688. doi: 10.1243/03093247jsa414
29. Pan B. Accurate, Fast, and Robust Digital Image Correlation. SPIE Newsroom; 2013. doi: 10.1117/2.1201307.005032
30. Grover DJ. Low-frequency drift reduction in the integration of repetitive signals. Proceedings of the Institution of Electrical Engineers. 1966; 113(5): 895–902. doi: 10.1049/piee.1966.0149
31. Castellini P, Paone N. Development of the tracking laser vibrometer: performance and uncertainty analysis. Review of Scientific Instruments. 2000; 71(12): 4639–4647. doi: 10.1063/1.1319862
32. Dorn C, Yang Y. Automated modal identification by quantification of high-spatial-resolution response measurements. Mechanical Systems and Signal Processing. 2022; 186: 109816. doi: 10.1016/j.ymssp.2022.109816
33. Deng T, Wang Y, Huang J, et al. Automatic high-resolution operational modal identification of thin-walled structures supported by high-frequency optical dynamic measurements. Materials. 2024; 17(20): 4999. doi: 10.3390/ma17204999
34. Li R, Zhang Y, Wang M, et al. Sparse strain sensing-based bending-torsion coupled deformation measurement in discontinuous stiffness open-hole CFRP panels using iFEM. Measurement Science and Technology. 2026; 37(4): 045207. doi: 10.1088/1361-6501/ae3b62
35. Yang S, Meng D, Alfouneh M, et al. A robust-weighted hybrid nonlinear regression for reliability based topology optimization with multi-source uncertainties. Computer Methods in Applied Mechanics and Engineering. 2025; 447: 118360. doi: 10.1016/j.cma.2025.118360
36. Meng D, Yang S, Jesus AMPD, et al. A novel hybrid adaptive Kriging and water cycle algorithm for reliability-based design and optimization strategy: application in offshore wind turbine monopile. Computer Methods in Applied Mechanics and Engineering. 2023; 412: 116083. doi: 10.1016/j.cma.2023.116083